KFUPM
Journal of Undergraduate Research International

Diamond Open Access 126

Article Mechanical Engineering/Physics

Comparative Study of Bio-Inspired and Ingenuity Airfoils at Martian Low Reynolds Numbers

Amro Alalfi and Mohamed Takeyeldein*

Cite https://doi.org/10.64589/juri/214393

Submitted: September 20, 2025 **Revised:** October 8, 2025 **Accepted:** November 18, 2025

ABSTRACT

Aerial flight on Mars introduces major aerodynamic challenges due to its thin atmosphere, resulting in low-Reynolds-number (Re) conditions where conventional airfoils undergo early flow separation and increased drag. This study evaluates and compares the performance of three airfoils: bio-inspired OWL, NASA's CLF5605, and AS6097, at Re = 23000, representative of Martian rotorcraft operations. Two turbulence models, k–ω SST and SST Transition, were tested using steady RANS CFD in ANSYS Fluent with dynamic similarity applied for terrestrial conditions. The SST Transition model showed better agreement with experimental results, particularly in capturing laminar separation bubbles. Among the airfoils, CLF5605 achieved the best aerodynamic efficiency, the OWL airfoil exhibited smooth aerodynamic trends and close validation agreement, and AS6097 produced the highest lift but inconsistent drag behavior.

Keywords: martian unmanned aerial vehicle, low reynolds number aerodynamics, bio-inspired airfoils, ingenuity helicopter, computational fluid dynamics simulation

1. INTRODUCTION

In recent years, engineers and scientists have progressively employed advanced technologies to push the boundaries of planetary exploration techniques, enabling missions that are more efficient, autonomous, and robust in extraterrestrial environments. Historically, these missions have been conducted using telescopes, rovers, and satellite technologies[1]. However, using rovers to explore Mars has presented difficulties owing to the rugged and rocky terrain, as well as limited mobility, prompting researchers to explore aerial exploration as a means to improve maneuverability and range of examination. Aerial flight under Martian conditions presents a significant aerodynamic challenge due to the planet's atmospheric composition, which is primarily carbon dioxide and has densities as low as 1% of those on Earth. These conditions result in a markedly reduced speed of sound, confining the airfoils and rotors to operate at low Reynolds number regimes, typically ranging between 10,000 and 25,000[1,2]. In this work, 'low Reynolds number' refers to the Re = 10,000–100,000 range relevant to small-scale rotorcraft and Martian flight conditions.

The low density of Mars reduces the lift generated by the rotor, necessitating higher RPMs to account for the decreased lift per blade area. Low Reynolds numbers increase the drag coefficient because of early flow separation and turbulent reattachment, creating a laminar separation bubble (LSB). Computational studies have shown that conventional airfoils have higher drag values due to early flow separation without reattachment, causing up to a 46% decrease in the maximum lift coefficient at low Reynolds numbers[3], whereas thin, highly cambered, and unconventional airfoils exhibit superior aerodynamic performance compared to thick symmetric airfoils[4]. In 2021, NASA's Ingenuity Mars Helicopter marked the first controlled extraterrestrial flight. This achievement was facilitated by its special airfoil design, which used thin, highly cambered airfoils to improve the lift at low Reynolds numbers and rounded leading edges to delay the separation of bubbles and enhance performance in laminar regimes[5].

Efforts to develop Martian aerial vehicles began with NASA's Mini-Sniffer program in 1977, followed by more agile UAV concepts such as the Y4TR in the 2010s[6]. These developments highlight the growing need for enhanced maneuverability and set the stage for adopting bio-inspired rotor designs, as birds and insects operate under low-Reynolds-number conditions in the Earth's atmosphere, allowing for higher lift-generating capabilities on Mars. Early experimental work[7] compared the aerodynamic performance of corrugated bio-inspired airfoils to conventional airfoils at Re = 34,000 using low-speed wind tunnels and high-resolution particle image velocimetry (PIV). The results indicated that bio-inspired airfoils exhibited no apparent flow separation up to high angles of attack compared to conventional airfoils and therefore achieved better aerodynamic coefficient values. The PIV analysis revealed that the improvement stemmed from delayed laminar separation bubble (LSB) formation and sustained attached flow at higher angles of attack, attributed to the thinner, highly cambered profile of the owl airfoil, which reduced the severity of adverse pressure gradients.

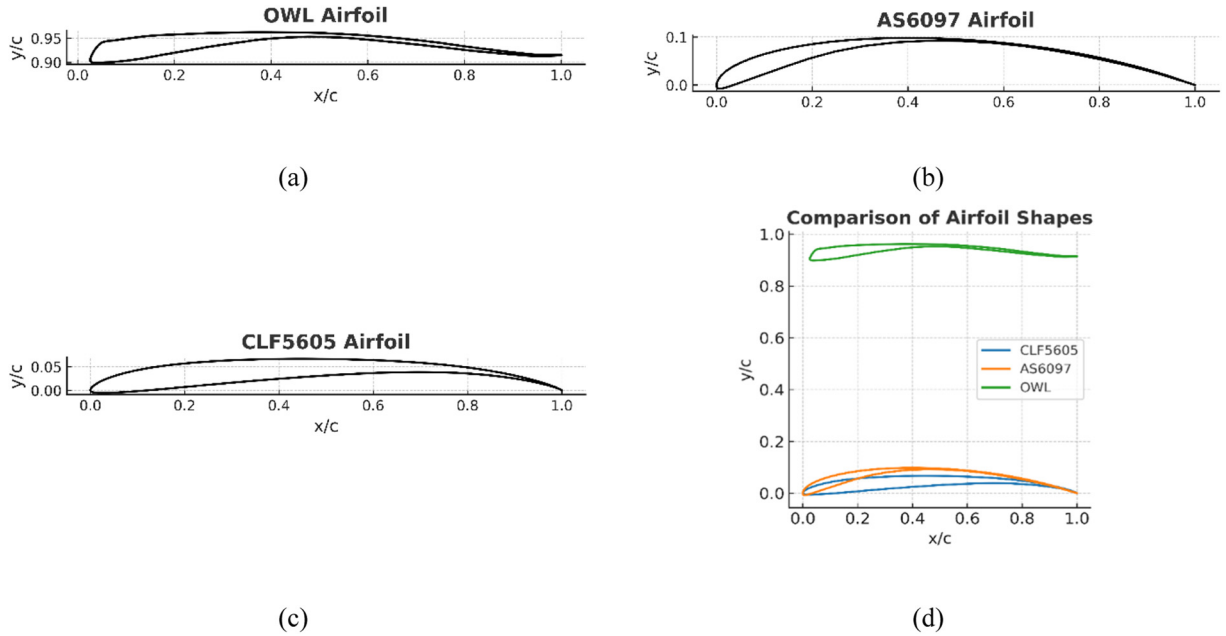

Figure 1. Airfoil geometries investigated at Martian low Reynolds numbers: (a) OWL airfoil; (b) AS6097; (c) CLF5605; and (d) comparison of the three profiles

Furthermore, multiple experiments[8,9] tested owl-inspired airfoils in a low-speed wind tunnel using force balance measurements across Reynolds numbers from 23,000 to 160,000, reporting up to a 6.7% improvement in the maximum lift compared to the NACA0012 airfoil. Several computational investigations[10–12] using both two-dimensional laminar computational fluid dynamics (CFD) and three-dimensional large-eddy simulation (LES) have consistently shown that owl-like airfoil geometries improve aerodynamic performance at low-Reynolds-number relative to canonical and other low-Re airfoils. Together, these studies demonstrate a common phenomenon: owl geometry produces strong suction peaks on the suction surface, controls the location and size of laminar separation bubbles (LSBs), and promotes pressure recovery, which increases the lift and reduces the drag over a broad range of angles of attack. When referenced collectively, these simulations provide robust evidence that tailoring camber, leading-edge radius, and upper-surface shape can deliberately manipulate LSB behavior to delay stall and enhance lift-to-drag ratio (L/D) for Re $\approx 10^4$.

Given the demonstrated superiority of bio-inspired airfoils at low Reynolds number flight regimes and the lack of research on their application in Martian conditions, this study aims to computationally evaluate the effectiveness of bio-inspired airfoils for Martian flights and benchmark their performance against NASA's Ingenuity airfoil. This research seeks to answer the following primary question: Can the flow control mechanisms inherent in bio-inspired airfoils, such as delayed separation, translate effectively to the specific compressibility and density constraints of the Martian atmosphere to outperform current state-of-the-art designs?

2. METHODOLOGY

2.1. Airfoil Selection. Three airfoils were used in this study, each selected for a specific purpose. NASA's CLF5605 airfoil was included as a benchmark to enable a comparison with the other test airfoils; its geometry was obtained from NASA documentation[5]. The Owl airfoil was chosen for its proven high-lift performance and delayed stall characteristics under low-Reynolds-number conditions, using the geometry defined by Liu et al.[13]. Finally, the AS6097 airfoil was selected as a bird-inspired profile featuring a favorable camber and leading-edge geometry to investigate the computational performance trends. Its geometry was sourced from Amanda and Selig[14].

2.2. Dynamic Similarity Setup. To replicate Martian low-Reynolds-number aerodynamics without introducing numerical instability, we employed the principle of dynamic similarity. The Martian operating Reynolds number (Re_M) was taken from the available literature: $Re_M = 23,000$, corresponding to Ingenuity's characteristic chord $c = 10$ cm[5]. Direct simulation using Martian atmospheric density ($\rho_M \approx 0.020$ kg/m^3) and viscosity ($\mu_M \approx 1.3 \times 10^{-5}$ kg/(m·s)) would result in prohibitively low freestream velocities and solver stiffness. Instead, all the CFD tests were performed under terrestrial air conditions, and the freestream velocity (V_E) was calculated as follows:

$$Re_E = \frac{\rho_E V_E c}{\mu_E} = Re_M \quad (1)$$

Because airfoil aerodynamics at low Mach numbers are primarily governed by the Reynolds number, this approach preserves the relevant dimensionless flow physics while avoiding the numerical challenge of simulating the Martian atmospheric conditions. To achieve a Reynolds number of 23,000 on a 10 cm chord airfoil in terrestrial conditions, assuming $\rho_E = 1.225$ kg/m^3 and $\mu_E = 1.81 \times 10^{-5}$ kg/(m·s), using Equation 1, we obtain $V_E \approx 3.4$ m/s. Since chord length is preserved and the Mach number remains well below 0.3 (M≈0.01M), compressibility effects are negligible, and Reynolds number governs the aerodynamic similarity. Consequently, the Earth-based CFD

simulations accurately reproduce the Martian low-Reynolds-number flow physics. Importantly, this approach also enables practical wind tunnel replication under the same velocity and chord length, allowing direct experimental validation with smoke visualization or PIV.

2.3. CFD Solver & Domain. To model the aerodynamics of the airfoils, a steady-state CFD solver was employed in ANSYS^{TM} Fluent software version 2022 R2; all numerical simulations were performed on a high-performance workstation equipped with an Intel Core i7 processor and 32 GB of RAM to ensure efficient convergence. A second-order upwind discretization scheme was used with SIMPLE pressure–velocity coupling, which is appropriate for steady incompressible flow, to enhance solver stability. Convergence was assessed by monitoring residuals (target 10^{-5}) and integrated force coefficients. Additionally, the lift and drag coefficients (C_L,C_D, respectively) were continuously monitored during each run to ensure stable convergence.

Turbulence modeling was necessary because flows at Re=23,000 lie within the laminar–transitional regime. Two models were tested: the k–ω model, selected for its robustness in predicting near-wall behavior and low-Reynolds-number flows, and the SST (Shear Stress Transport) four-equation model, adopted for its improved ability to resolve separation bubbles and transitional phenomena, which are critical at low Reynolds numbers.

The governing equations solved were the steady, incompressible Navier–Stokes equations with Reynolds-averaged turbulence closure:

$$\nabla \cdot \vec{u} = 0 \tag{2}$$

$$\rho(\vec{u} \cdot \nabla)\vec{u} = -\nabla p + \mu \nabla^2 \vec{u} + \overrightarrow{F_{turb}} \tag{3}$$

where $\mathbf{F_{turb}}$ is the modeled Reynolds stress contribution from the turbulence models.

A C-type computational domain was adopted, with Farfield boundaries sufficiently distant from the airfoil to avoid blockage. The angle of attack (AoA) was varied from -2° to 12° in increments of 2°. The inlet conditions were set at V_E =3.4 m/s (from the dynamic similarity analysis), whereas the outlet was prescribed with zero static gauge pressure. The airfoil surface was modelled as a no-slip wall.

An unstructured mesh (Figure 2) with approximately 150,000 cells was generated, with strong refinement near the airfoil wall to resolve laminar separation bubbles, incorporating at least 30 inflation layers and targeting a near-wall resolution of $y^+ \approx 10^{-5}$. Mesh quality was maintained with skewness <0.25 and orthogonal quality >0.95, ensuring solver robustness. Table 1 summarizes the CFD setup and settings used in this study. Since this study relies entirely on computational fluid dynamics simulations of inanimate airfoil geometries and involves no human or animal subjects, specific ethical approval or informed consent was not required.

3. RESULTS AND DISCUSSION

3.1. Results.

3.1.1. Aerodynamic coefficients. Figure 3 compares the aerodynamic performance of the AS6097, OWL, and CLF5605 airfoils in terms of lift coefficient (C_L), drag coefficient (C_D), and lift-to-drag ratio (C_L/C_D) as predicted by the k–ω SST and SST Transition turbulence models over a range of angles of attack (AOA).

For the AS6097 airfoil, both turbulence models showed significant overlap in the prediction of the lift coefficient up to an AOA of 6°, after which some differences were observed past that point. The lift coefficient peaked around an AOA of 10° before exhibiting stall behavior. The drag calculation coefficient exhibited significant fluctuations in both models, with a sharp decrease at an AOA of 6°. Specifically, the k-ω SST model predicted a

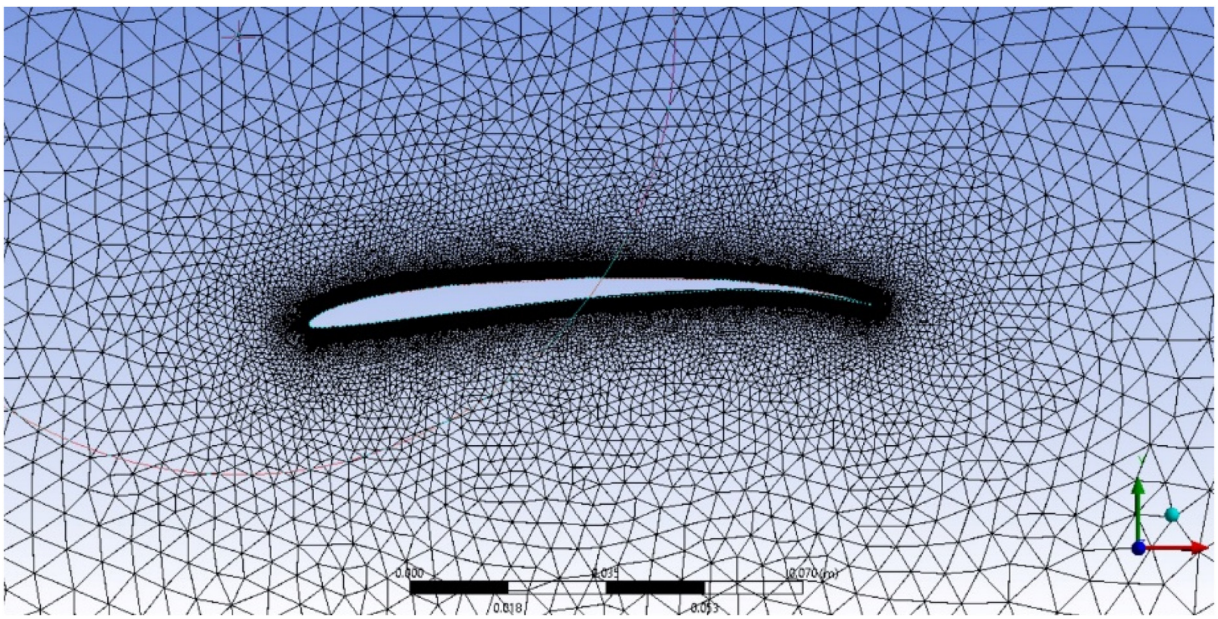

Figure 2. Unstructured triangular mesh with inflation layers around the airfoil surface

Table 1. *CFD setup*

Parameter	Specification
Solver	ANSYS Fluent, pressure-based, steady-state
Governing equations	Incompressible URANS (continuity + momentum)
Discretization	Second-order upwind for momentum & turbulence equations
Pressure–velocity coupling	SIMPLE algorithm
Convergence criteria	Residuals $<10^{-5}$; stable C_L, C_D, C_L/C_D monitoring
Turbulence models	1. Standard k–ω (robust near-wall, adverse pressure gradients) 2. Transition SST (for laminar–transitional flows)
Boundary conditions	Inlet velocity V_E =3.4 m/s; outlet static pressure = 0 Pa; airfoil = no-slip wall
Angle of Attack range	−2° to 12°, step = 2°
Meshing strategy	Unstructured grid with refinement near airfoil; ≥ 30 inflation layers; $y^+ \approx 10^{-5}$
Grid independence	3 progressively refined meshes tested; outputs compared for independence
Validation	CLF5605 and OWL vs. published data; AS6097 vs. XFOIL at the same Re

C_D of approximately 0.08, while the SST Transition model predicted a significantly lower C_D of approximately 0.06 at this angle of attack. This sharp decrease in drag, followed by a subsequent increase, led to a spike in C_L/C_D at the same AOA. While AS6097 achieved the highest maximum lift coefficient (CLmax) its drag performance was inconsistent, an effect attributed to the formation of laminar separation bubbles.

For the OWL airfoil, both models exhibited similar aerodynamic coefficients throughout the AOA range. The lift coefficient consistently increased up to the highest measured AOA of 12°, when it began to show signs of stall. A small difference in C_L/C_D was noted between AOA of 6° and 10°. A maximum C_L of approximately 1.2 is achieved at an AOA of 12°. Overall, the OWL airfoil showed the smoothest and most predictable trends, making it suitable for stable applications.

The CLF5605 airfoil also exhibited consistent aerodynamic coefficients in both models within the range of AOAs, with only minor differences. Its maximum lift coefficient was slightly lower than that of the other two airfoils, peaking at approximately 1.1 near AOA of 12°. Both turbulence models showed consistent flow behavior and aerodynamic coefficient predictions with some differences in magnitude, most notably in the calculation of the drag force on AS6097. AS6097 had the highest lift force, peaking at a C_L of approximately 1.4, whereas CLF5605 had the best aerodynamic efficiency, reaching a peak C_L/C_D of >20.

Overall, the SST Transition model provides a more conservative drag prediction and slightly different stall behavior, while the k–ω SST model predicted higher aerodynamic efficiency. Among the airfoils tested, CLF5605 consistently exhibited a superior lift-to-drag performance, highlighting its aerodynamic advantages under low-Reynolds-number conditions.

3.1.2. Grid independence study. To validate these results, a grid convergence study was conducted to ensure that the solver results were not biased at higher mesh densities. This was done by selecting a representative case, running the solver at different inflation layers, and then comparing the resulting aerodynamic coefficients with different pressure-velocity coupling schemes. The CLF5606 airfoil at an angle of attack of 6° was selected, and the simulations were performed on inflation layers ranging from 30 to 70. The results are shown in Table 2.

The SIMPLE solver was employed for all simulations to improve solver stability. The grid-independence study demonstrated excellent convergence with this solver, as shown in Table 2. For completeness, the coupled solver was also tested and showed similar convergence behavior, with the final values differing by less than 0.4% from the SIMPLE solver results at 70 inflation layers, validating the overall approach.

3.1.3. Validation. The comparison of the lift, drag, and lift-to-drag ratio for the OWL airfoil at Re=23000 in Figure 4 demonstrates that both turbulence models captured the expected aerodynamic behavior and showed good agreement with the reference study by Anyoji (2018). The k–ω SST model slightly overpredicted lift at low angles of attack due to its fully turbulent assumption, while the SST Transition model provides a more realistic pre-stall slope by accounting for laminar–turbulent transition. Both models, however, underpredicted the experimentally observed maximum lift. In drag prediction, both approaches underestimate the values across the range of angles; however, the SST Transition model yields slightly higher drag values that more closely align with the reference data, particularly in the pre-stall regime, where laminar separation bubbles dominate. Consequently, the computed aerodynamic efficiency (C_L/C_D) was somewhat higher than that of the reference data; however, the overall variation with the AOA was well reproduced. It is worth noting that part of the discrepancy may stem from slight geometric differences between the Liu et al. owl-like airfoil configuration used in this study and the test model used by Anyoji et al., as highlighted in their study. Nevertheless, the results demonstrate very good overall agreement, with the SST Transition model showing improved fidelity at this low Reynolds number, while the standard k–ω SST provides a sharper stall prediction.

Figure 5 presents the validation of the CFD predictions against the experimental data for the CLF5605 airfoil at Re = 23,000 under two-dimensional flow conditions. The experimental datasets were sourced from wind tunnel campaigns conducted in Japan and the United States [15]. The computational results were

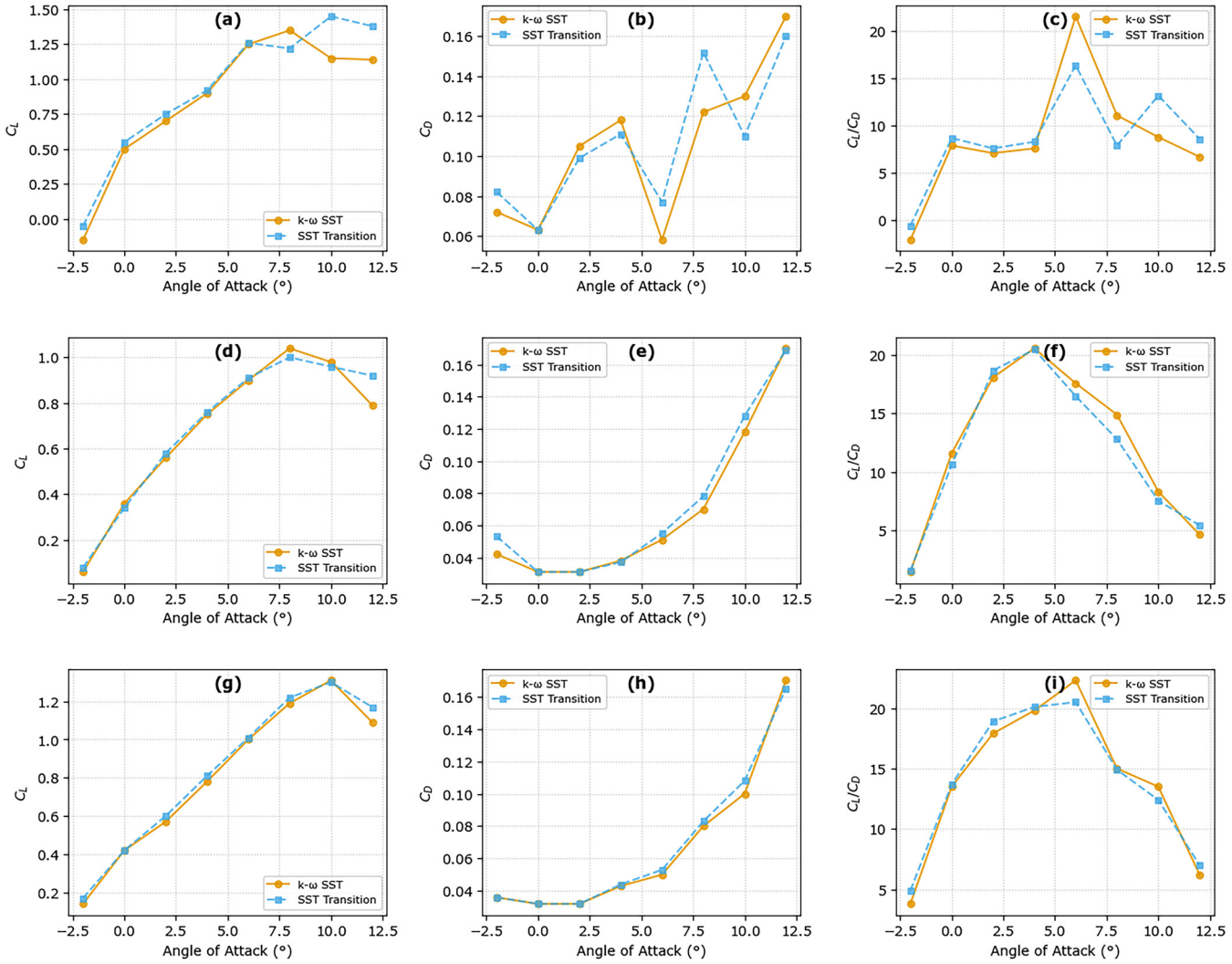

Figure 3. Comparative aerodynamic performance of AS6097, OWL, and CLF5605 airfoils under k–ω SST and SST Transition models. (a–c) AS6097: lift, drag, and lift-to-drag ratio vs. angle of attack.(d–f) OWL: lift, drag, and lift-to-drag ratio vs. angle of attack.(g–i) CLF5605: lift, drag, and lift-to-drag ratio vs. angle of attack

obtained using steady RANS simulations with both the k–ω SST model and the SST four-equation transition model.

The lift curves showed good agreement across all datasets, with the CFD models reproducing both the slope and stall onset. The maximum lift coefficient predicted by CFD ($C_{Lmax} \approx 1.32$–1.34) fell within the range of the experimental data, though slightly underpredicting the highest values observed in the Japanese dataset[15]. The minimum drag coefficient from the simulations is $C_{Dmin} \approx 0.031$–0.032, somewhat lower than the experimental drag polars, leading to an optimistic prediction of aerodynamic efficiency. The maximum lift-to-drag ratios are $C_L/C_{Dmax} \approx 22.0$ (SST) and 20.4 (SST transition), compared with lower values in the experiments, which reflects the RANS tendency to underpredict viscous drag at low Reynolds numbers.

Discrepancies in drag are expected because of the inability of RANS closures to accurately capture laminar separation bubbles, transition onsets, and small-scale unsteadiness, which dominate low-Reynolds airfoil aerodynamics. This effect is especially

Table 2. *Grid Independence Study*

	Coupled			SIMPLE		
Inflation layers	**C_L**	**C_D**	**C_L/C_D**	**C_L**	**C_D**	**C_L/C_D**
30	1.1000	0.05400	20.3704	1.0705	0.0475	22.5368
40	1.1120	0.05410	20.5545	1.1117	0.0502	22.1665
55	1.1266	0.05390	20.9017	1.1257	0.0540	20.8463
60	1.1230	0.05400	20.7963	1.1299	0.0538	21.0173
70	1.1322	0.05320	21.2820	1.3200	0.0532	21.1984

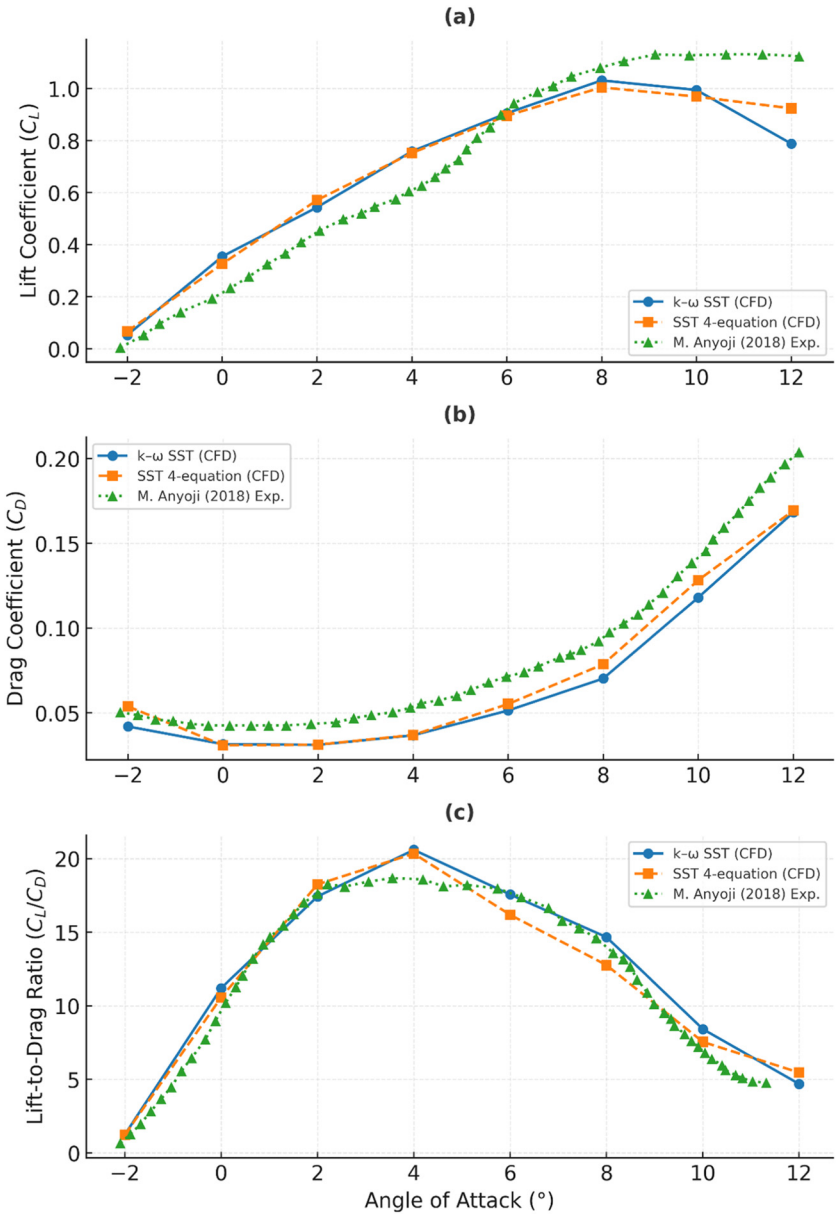

Figure 4. Aerodynamic coefficients for the OWL airfoil using $k-\omega$ SST (CFD), SST 4-equation (CFD), and M. Anyoji (2018) experimental data at Re = 23000. (a) Lift coefficient (C) vs. angle of attack.(b) Drag coefficient (C_d) vs. angle of attack. (c) Lift-to-drag ratio (C_l/C_d) vs. angle of attack

pronounced in the drag, as even minor errors in modeling the transition location can significantly alter the boundary-layer development. Nevertheless, the CFD results reproduced the main aerodynamic trends and provided credible predictions of the lift, stall behavior, and overall performance envelope, validating their use for further analysis. The primary objectives of this study—to computationally benchmark bio-inspired airfoils (OWL, AS6097) against the Ingenuity airfoil (CLF5605) and validate the CFD models against experimental data—were successfully met. The results provide a clear comparison of aerodynamic performance and modeling fidelity under the specified low-Reynolds-number conditions.

3.2. Discussion. This study drew multiple comparisons between different airfoil designs, turbulence models, and validation datasets to investigate the aerodynamic behavior under Martian Reynolds number conditions. Having presented the detailed results, it is now appropriate to take an overall view to draw broader conclusions and consolidate our understanding of the problem.

Two turbulence models were primarily employed to evaluate the predictive capability. The k–ω SST model performed well in predicting the lift coefficient (C_L) in the pre-stall regime but consistently overpredicted the drag coefficient (C_D) and deviated from complementary computational reference results at higher angles of attack. In contrast, the SST Transition model produced results more consistent with the validation datasets and demonstrated better capability in predicting turbulent reattachment in the pre-stall region. At low angles of attack, both models produced highly similar results, but as the angle of attack increased, the k–ω SST predictions began to deviate, reinforcing the SST Transition model as the more reliable choice at these Reynolds number conditions.

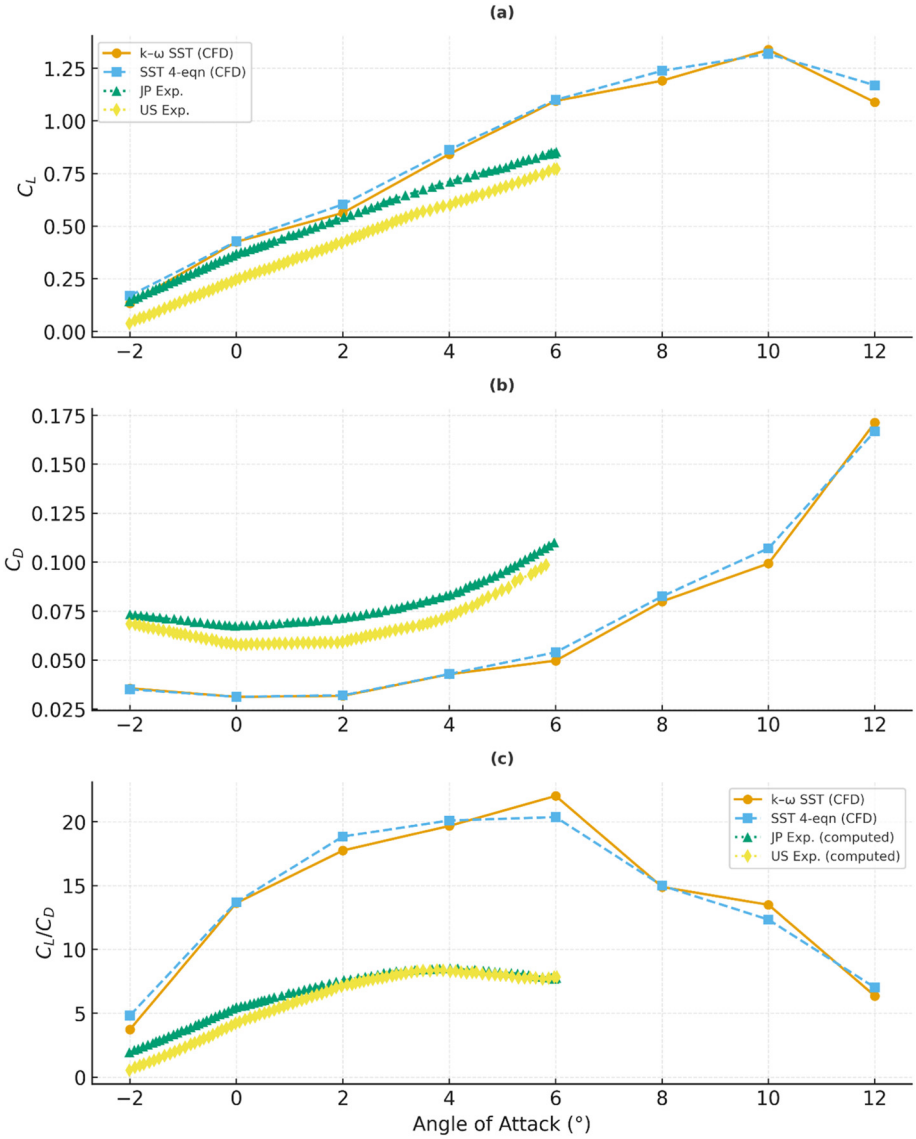

Figure 5. Aerodynamic coefficients using k–ω SST (CFD), SST 4-equation (CFD), JP Exp., and US Exp. Datasets at Re = 23000. (a) Lift coefficient (C_L) vs. angle of attack. (b) Drag coefficient (C_D) vs. angle of attack. (c) Lift-to-drag ratio (C_L/C_D) vs. angle of attack

Three airfoil configurations were tested: an OWL-like airfoil, NASA CLF5605, and AS6097. Among them, the CLF5605 exhibited the most aerodynamic efficiency, confirming its suitability and explaining its selection for NASA's Ingenuity Mars helicopter. The OWL airfoil also showed a smooth and predictable aerodynamic response and closely matched the validation datasets, suggesting its potential for stable and efficient low-Reynolds-number applications. AS6097 achieved the highest maximum lift coefficient (C_{Lmax}) among the three but produced inconsistent drag values, likely due to the formation of laminar separation bubbles. This behavior suggests the formation and reattachment of a laminar separation bubble, a phenomenon that the SST Transition model is specifically designed to capture. This airfoil could not be validated against literature data, as no comparable CFD or experimental studies were found, indicating that its performance requires further investigation.

The grid independence study confirmed that the selected mesh was sufficiently refined to resolve the aerodynamic features without introducing grid-related artifacts, ensuring that the observed differences stemmed from physical modeling rather than numerical errors.

For validation, the CLF5605 case provides a detailed comparison with wind tunnel experiments conducted in Japan and the United States. Both turbulence models captured the lift behavior and stall onset accurately. The simulations predicted $C_{Lmax} \approx 1.34$ (k–ω SST) and 1.32 (SST Transition), values within the experimental range. The minimum drag coefficients were predicted as $C_{Dmin} \approx 0.031$–0.032, slightly lower than measured experimentally, leading to optimistic lift-to-drag ratios ($C_L/C_{Dmax} \approx 22.0$ for SST and 20.4 for SST Transition). The Japanese and U.S. experimental datasets exhibited minor differences, reflecting the sensitivity of low-Reynolds-number airfoil aerodynamics to wind tunnel conditions such as turbulence intensity, surface roughness, and wall effects. The fact that CFD predictions fell within this experimental range adds confidence to the overall results.

Collectively, these findings highlight several important points. At Martian Reynolds numbers, small discrepancies in drag

prediction lead to disproportionately large variations in aerodynamic efficiency (CL/CD), which is critical for vehicle performance. Although steady RANS models provide reliable predictions of the lift and stall onset, their drag prediction ability is limited by the simplified treatment of laminar separation bubbles, transition onset, and unsteady vortex dynamics. The SST Transition model reduces some of these errors by accounting for transition effects; however, higher-fidelity methods may be required for more accurate efficiency predictions.

As noted in the results, the numerical behavior of the airfoils at Re $\approx$ 23,000 suggests the formation and reattachment of a laminar separation bubble (LSB). This phenomenon is a critical point of uncertainty for the present study. The quantitative CD and CL values derived from the 2D RANS models must be interpreted with a clear understanding of the known limitations of these models in the low–Reynolds-number, transitional regime. The k–omega SST model, in particular, is known to struggle with this flow physics.

A recent high-fidelity benchmark study[16] directly compared 2D RANS k–omega SST simulations against experimental Particle Image Velocimetry (PIV) data for an airfoil with complex flow separation. The findings were stark: the RANS model failed to capture the true extent of the separation, resulting in a 58% error in the predicted drag coefficient (CD) and a 78% error in the lift coefficient (CL). The study diagnosed this failure as the RANS model's tendency to overestimate turbulent mixing near the wall, which artificially energized the boundary layer and prevented the physical separation that the PIV data clearly measured.

This finding is directly relevant to our Martian airfoil investigation. It implies that our RANS-predicted CD values are likely under-predicted, and the true size and behavior of the LSBs are not fully resolved.

For design applications, the results suggest that CLF5605 and OWL airfoils are the most promising candidates for Martian low-Reynolds-number flights. CLF5605 stands out for its proven efficiency and prior successful application, while the OWL configuration shows potential as a stable and predictable alternative. AS6097, although capable of producing a high lift, requires further investigation due to its inconsistent drag behavior.

Finally, this study emphasizes the importance of turbulence modeling accuracy in low-Reynolds-number aerodynamic. Future work could extend this research by employing large-eddy simulations (LES) or hybrid RANS/LES methods to better capture the laminar separation and transition phenomena. Additionally, quasi-2D or 3D wind tunnel tests with transition location measurements would provide valuable benchmarks for further validation. The study also assumed a rigid airfoil and did not model aeroelastic effects, such as the blade flapping or twisting that could occur under aerodynamic loads on a flexible Martian rotor. Together, these efforts would strengthen the predictive capability and support the development of efficient Martian aerial platforms.

4. CONCLUSIONS

This study explored the aerodynamic performance of the OWL, CLF5605, and AS6097 airfoils under Martian conditions using CFD to compare the performance of the k–ω SST and SST Transition turbulence models. Several key conclusions were drawn.

1. Modeling Fidelity and Limitations: This work confirms that selecting a transition-sensitive turbulence model (SST Transition) is critical for capturing low-Re flow physics. However, the study also reinforces that even advanced RANS models underpredict drag. This discrepancy, attributed to RANS limitations in resolving laminar separation bubbles, confirms that RANS is a reliable tool for predicting lift and stall but not for final drag and performance-efficiency calculations.Future work: High-fidelity CFD methods (LES and hybrid RANS–LES) and quasi-2D or 3D wind tunnel studies with transition measurements are recommended to refine the predictive accuracy and support rotorcraft design optimization for Martian environments.
2. Airfoil Performance Insights: While the benchmark CLF5605 was validated as the most aerodynamically efficient, the bio-inspired OWL airfoil proved to be a highly stable and reliable alternative. The AS6097, conversely, demonstrated that high lift can be negated by LSB-induced drag inconsistencies, proving that bio-inspired geometry alone is not a guarantee of superior performance.

Overall, this study's primary contribution is twofold. From a practical standpoint, it provides aerospace engineers with a direct performance comparison, validating the CLF5605's efficiency while qualifying the OWL airfoil as a viable alternative for future Martian rotorcraft. From a theoretical standpoint, the findings underscore that at Martian Reynolds numbers (Re $\approx 2.3 \times 10^4$), the mitigation of laminar separation bubbles becomes the dominant design driver, often proving more critical for aerodynamic efficiency than high-lift profiling alone.

AFFILIATIONS AND AUTHOR DETAILS

Undergraduate Authors

Amro Alalfi – *Aerospace Engineering, King Fahd University of Petroleum and Minerals, Dhahran 31261, Saudi Arabia;* 0009-0005-9299-5504
Email: s202254140@kfupm.edu.sa

Corresponding Author

Mohamed Takeyeldein – *Research Mentor, Interdisciplinary Research Center for Aviation and Space Exploration, King Fahd University of Petroleum and Minerals Dhahran 31261, Saudi Arabia;* 0000-0002-6888-0783
Email: mohamed.elsayed@kfupm.edu.sa

ACKNOWLEDGEMENTS

The authors would like to express their sincere gratitude to the King Fahd University of Petroleum and Minerals (KFUPM) and the Department of Aerospace Engineering for their support.

REFERENCES

(1) Withrow, S. *et al.* Mars Science Helicopter Conceptual Design. in *ASCEND 2020* (American Institute of Aeronautics and Astronautics, Reston, Virginia, 2020). doi:10.2514/6.2020-4029.

(2) Giacomini, E. & Westerberg, L.-G. Rotorcraft Airfoil Performance in Martian Environment. *Aerospace* **11**, (2024).

(3) Winslow, J., Otsuka, H., Govindarajan, B. & Chopra, I. Basic Understanding of Airfoil Characteristics at Low Reynolds Numbers (104–105). *J. Aircr.* **55**, 1050–1061 (2018).

(4) Menon, K. & Mittal, R. Aerodynamic Characteristics of Canonical Airfoils at Low Reynolds Numbers. *AIAA J.* **58**, 977–980 (2020).

(5) Koning, W. J. F. & Dominguez, M. *Mars Helicopter Ingenuity Rotor Geometry*. http://www.sti.nasa.gov (2024).

(6) Hassanalian, M., Rice, D. & Abdelkefi, A. Evolution of space drones for planetary exploration: A review. *Prog. Aerosp. Sci.* **97**, 61–105 (2018).

(7) Hu, H. & Tamai, M. Bioinspired Corrugated Airfoil at Low Reynolds Numbers. *J. Aircr.* **45**, 2068–2077 (2008).

(8) Anyoji, M., Wakui, S., Hamada, D. & Aono, H. Experimental Study of Owl-Like Airfoil Aerodynamics at Low Reynolds Numbers. *J. Flow Control. Meas. & Vis.* **06**, 185–197 (2018).

(9) Kazemi, M. & Mani, M. Owl airfoil aerodynamic noise sources and performance compared to hawk and NACA0012 airfoils for low Reynolds applications. *Sci. Rep.* **15**, 23261 (2025).

(10) KONDO, K. *et al.* Analysis of Owl-like Airfoil Aerodynamics at Low Reynolds Number Flow. *Trans. JAPAN Soc. Aeronaut. Sp. Sci. Aerosp. Technol. JAPAN* **12**, Tk_35-Tk_40 (2014).

(11) AONO, H. *et al.* Aerodynamics of Owl-like Wing Model at Low Reynolds Numbers. *Trans. Jpn. Soc. Aeronaut. Space Sci.* **63**, 8–17 (2020).

(12) Kondo, K. *et al.* Large-Eddy Simulations of Owl-Like Wing Under Low Reynolds Number Conditions. in (American Society of Mechanical Engineers, 2013). doi:10.1115/FEDSM2013-16377.

(13) Liu, T., Kuykendoll, K., Rhew, R. & Jones, S. Avian Wing Geometry and Kinematics. *AIAA J.* **44**, 954–963 (2006).

(14) Ananda, G. K. & Selig, M. S. Design of Bird-Like Airfoils. in *2018 AIAA Aerospace Sciences Meeting* (American Institute of Aeronautics and Astronautics, Reston, Virginia, 2018). doi:10.2514/6.2018-0310.

(15) Koning, W. J. F. *et al. Experimental Results for Mars Rotorcraft Airfoils (Roamx-0201 and Clf5605) at Low Reynolds Number and Compressible Flow in a Mars Wind Tunnel*. https://ntrs.nasa.gov/citations/20240004230 (2024).

(16) Gutierrez, R., Zamponi, R., Ragni, D., Llorente, E. & Aranguren, P. On the extension of kωSST corrections to predict flow separation on thick airfoils with leading-edge roughness. *Wind Energy* **26**, 650–667 (2023).